

## Article (refereed) - postprint

---

Cox, Peter M.; Huntingford, Chris; Williamson, Mark S. 2018. **Emergent constraint on equilibrium climate sensitivity from global temperature variability.** *Nature*, 553 (7688). 319-322. <https://doi.org/10.1038/nature25450>

© 2018 Macmillan Publishers Limited, part of Springer Nature

This version available <http://nora.nerc.ac.uk/id/eprint/519612/>

NERC has developed NORA to enable users to access research outputs wholly or partially funded by NERC. Copyright and other rights for material on this site are retained by the rights owners. Users should read the terms and conditions of use of this material at

<http://nora.nerc.ac.uk/policies.html#access>

**This is a post-peer-review, pre-copyedit version of an article published in *Nature*, 553 (7688). 319-322. The final authenticated version is available online at: <http://dx.doi.org/10.1038/nature25450>.**

**There may be differences between this version and the publisher's version. You are advised to consult the publisher's version if you wish to cite from this article.**

Contact CEH NORA team at  
[noraceh@ceh.ac.uk](mailto:noraceh@ceh.ac.uk)

# Emergent constraint on equilibrium climate sensitivity from global temperature variability

Peter M. Cox<sup>1</sup>, Chris Huntingford<sup>2,1</sup> Mark S. Williamson<sup>1</sup>

<sup>1</sup> College of Engineering, Mathematics and Physical Science, University of Exeter, EX4 4QF, UK

<sup>2</sup> Centre for Ecology and Hydrology, Wallingford, Oxon OX10 8BB, UK

**Equilibrium Climate Sensitivity (*ECS*) remains one of the most important unknowns in climate change science. *ECS* is defined as the global mean warming that would occur if the atmospheric carbon dioxide concentration was doubled and the climate was brought to equilibrium with that new level of CO<sub>2</sub>. Despite its rather idealised definition, *ECS* has continuing relevance for international climate change agreements, which are often framed in terms of the stabilisation of global warming relative to the pre-industrial climate. However, the ‘likely’ range of *ECS* as stated by the Intergovernmental Panel on Climate Change (IPCC) has remained at 1.5-4.5K for more than 25 years<sup>1</sup>. The possibility of a value of *ECS* towards the upper end of this range reduces the feasibility of avoiding 2K of global warming. Here, we present a new ‘Emergent Constraint’ on *ECS* which yields a central estimate of *ECS*=2.8K with 66% confidence limits (equivalent to the IPCC ‘likely’ range) of 2.2-3.4K. Our approach is to focus on the variability of temperature about the long-term historical warming, rather than on the warming trend itself. We use an ensemble of climate models to define an emergent relationship<sup>2</sup> between the *ECS*, and a theoretically-informed metric of global temperature variability. This metric of variability can also be calculated from observational records of global warming<sup>3</sup>, which enables tighter constraints to be placed on *ECS*, reducing the probability of *ECS*<1.5K to less than 3%, and the probability of *ECS*>4.5K to less than 1%.**

Many attempts have been made to constrain *ECS*, typically utilising either the record of historical warming or reconstructions of past climates<sup>4</sup>. Methods based on the historical warming are affected by uncertainties in ocean heat uptake and the contribution of aerosols to net radiative forcing<sup>5,6</sup>. These methods also diagnose the effective climate sensitivity over the historical period which may be different to the *ECS*, due to the strength of climate feedbacks varying with the evolving pattern of surface temperature change<sup>4,7,8,9</sup>. Although methods based on past climates, such as the last glacial maximum<sup>10</sup>, are more closely related to the concept of equilibrium, they suffer instead from even larger uncertainties in the reconstruction of net radiative forcing.

As an alternative, the Emergent Constraint approach uses an ensemble of complex Earth System Models to estimate the relationship between a modelled but observable variation in the Earth System and a predicted future change<sup>2,11</sup>. The model-derived emergent relationship can then be combined with the quantification of the observed variation to produce an ‘emergent constraint’ on the predicted future change<sup>2,11,12</sup>. This paper presents an Emergent Constraint on *ECS*, based on the variability of global-mean temperature.

In order to inform our search for an emergent constraint, we consider the simple ‘Hasselmann Model’<sup>13</sup> for the variation in global mean temperature ( $\Delta T$ ) in response to a radiative forcing ( $Q$ ):

$$C \frac{d\Delta T}{dt} = Q - \lambda \Delta T = N \quad (1)$$

The single heat capacity ( $C$ ) in this model is a simplification that is known to be a poor representation of ocean heat uptake on longer timescales<sup>14,15,16</sup>. However, we find that it still offers very useful guidance about global temperature variability on shorter timescales. The climate feedback factor ( $\lambda$ ) determines how the net top-of-atmosphere planetary energy balance ( $N$ ) varies with temperature change ( $\Delta T$ ) in response to a radiative forcing change ( $Q$ ). *ECS* and  $\lambda$  are inversely related, with a constant of proportionality which is the radiative forcing due to doubling of atmospheric CO<sub>2</sub>,  $Q_{2\times\text{CO}_2}$ :  $ECS = Q_{2\times\text{CO}_2}/\lambda$ . Although the diagnosed  $Q_{2\times\text{CO}_2}$  varies across the model ensemble<sup>17</sup>, the uncertainty in *ECS* is predominately due to uncertainty in  $\lambda$ , which varies from 0.6 to 1.8 W m<sup>-2</sup> K<sup>-1</sup>, as shown in Table ED1.

If  $Q$  can be approximated as white-noise forcing with variance  $\sigma_Q^2$ , the Hasselmann model can be solved to give expressions for the variance ( $\sigma_T^2$ ) and the one year-lag autocorrelation of the global temperature ( $\alpha_{1T}$ ), which can be combined to yield an equation for *ECS* (see Methods):

$$ECS = \sqrt{2} Q_{2\times\text{CO}_2} \left\{ \frac{\sigma_T}{\sigma_Q} \right\} \frac{1}{\sqrt{-\log_e \alpha_{1T}}} = \sqrt{2} \frac{Q_{2\times\text{CO}_2}}{\sigma_Q} \Psi \quad (2)$$

where  $\Psi = \sigma_T/\sqrt{-\log_e \alpha_{1T}}$  is the key metric of global temperature variability. This equation is essentially a fluctuation-dissipation relationship<sup>18</sup> relating the variability of the climate ( $\sigma_Q, \sigma_T, \alpha_{1T}$ ) to its sensitivity to external forcing (*ECS*).

Observational records of global mean temperature change<sup>3</sup> enable  $\Psi$  to be estimated for the real world. The variance of the net radiative forcing is approximately equal to the variance of the top-to-the-atmosphere flux ( $\sigma_N^2$ ), which can in principle be estimated from satellite measurements.

However, the available satellite records are currently too short to provide reliable estimates of  $\sigma_N$ . In addition, the radiative forcing due to doubling  $\text{CO}_2$  ( $Q_{2\times\text{CO}_2}$ ) is not observable in the real world. This means that the right-hand-side of Equation (2) cannot be directly estimated from observations. Fortunately, we find that the variation in  $ECS$  is weakly correlated with  $Q_{2\times\text{CO}_2}/\sigma_N$  across the model ensemble (see Table ED1). We can therefore approximate the predicted gradient of the  $ECS$  versus  $\Psi$  emergent relationship using the ensemble mean value of  $Q_{2\times\text{CO}_2}/\sigma_N$  ( $=8.7$ ). Our theory therefore predicts a gradient of the  $ECS$  versus  $\Psi$  emergent relationship of  $8.7\sqrt{2} = 12.2$ .

Figure 1(a) shows the simulation of global warming in the historical simulations with the 16 models in the CMIP5 ensemble<sup>19,20</sup> used here (see list in Table ED1). Here and throughout, higher-sensitivity models ( $\lambda < 1.0 \text{ W m}^{-2} \text{ K}^{-1}$ ) are shown in magenta, and lower sensitivity models ( $\lambda > 1.0 \text{ W m}^{-2} \text{ K}^{-1}$ ) are shown in green. Observations from the HadCRUT4 dataset<sup>3</sup> are shown by the black line marked with dots. Figure 1(a) illustrates that both high and low sensitivity models are able to fit the historical record with reasonable fidelity, despite implying very different future climates. Models with higher  $ECS$  values also have longer response times, and there are variations across the models in net radiative forcing and in ocean heat uptake - allowing models with both high and low sensitivities to reproduce historical global warming<sup>21</sup>. As a result, the fit to the global temperature record does not provide a direct constraint on  $ECS$ , as shown in Figure 1(b).

In order to test whether variability is a better constraint on  $ECS$ , we de-trend the global mean temperature records from the models and the observations. Our approach to de-trending is informed by techniques designed to detect precursors of potential tipping-points<sup>22</sup> such as ‘critical slowing down’<sup>23</sup>. The method applied in that case is to use a moving window, to linearly de-trend within that window, and then to calculate statistics of the de-trended residuals. For tipping point detection, the favoured variable is often the lag-1 autocorrelation which measures the memory in fluctuations of the analysed variable<sup>23</sup>. We use a similar approach, although here we apply it to analyse the relationship between  $\Psi$  and  $ECS$  across the ensemble of models, rather than to detecting declining system resilience in a single realisation of the system.

We analyse the annual-mean global-mean temperature time-series from 16 CMIP5 historical simulations and compare to the HadCRUT4 observational dataset. Although there were another 23 historical runs available in the CMIP5 archive, we chose to use just one model variant from each climate centre, to avoid biasing the emergent constraint towards the centres with the most model runs in the archive. Where there was more than one model variant from a modelling centre, we took the model variant from that centre that had the smallest RMS error in the fit to the record

of observed global warming from 1860 to 2016. The remaining 23 model runs (which included some initial condition ensembles) were subsequently used to test the robustness of the emergent constraint (see Figure ED1).

Figure 2a shows the resulting variation in  $\Psi$  for each of the models and the observations, using a window width of 55 years, and data from 1880 to 2016 to match the available observational datasets. Although  $\Psi$  varies in time, the different models are clearly distinguished, in contrast to the simulations of historical global warming (Figure 1a). In particular, the  $\Psi$  values separate higher-sensitivity models (magenta lines) from lower-sensitivity model (green lines), with higher sensitivity models producing larger  $\Psi$  values. It is also worth noting at this point that  $\Psi$  from the observational data is within the range of the lower-sensitivity models but clearly outside the range of the higher-sensitivity models. Figure 2b shows the emergent relationship between  $ECS$  and the time-mean  $\Psi$  values across the model ensemble. The vertical blue lines show the observational constraint on  $\Psi$  from the HadCRUT4 dataset, but similar observational constraints are also derived from other datasets of global mean temperature (see Table ED2).

As in previous studies<sup>11,12</sup> the emergent relationship from the historical runs and observational constraint can be combined to provide an emergent constraint on  $ECS$ . This involves convoluting the prediction error implied by the fit of the scatter plot to the emergent relationship, with the uncertainty in the observations, to produce a probability density function (PDF) for the y-axis variable (see online Methods). Figure 3(a) shows the resulting PDF for  $ECS$  (black curve). For comparison, the prior PDF implied by the equal-weighted model ensemble is shown by the orange histogram. The emergent constraint PDF is sharply peaked around a best-estimate of  $ECS=2.8$  K, which is slightly smaller than the centre of the IPCC range of 1.5-4.5K. Our best-estimate of  $ECS$  is considerably larger than the values derived from raw energy budget constraints<sup>8,24,25</sup> but similar to some recent estimates that account for time-dependent and forcing-dependent feedbacks<sup>9,26</sup>.

Figure 3(b) shows the resulting cumulative density function (CDF) which gives the probability of  $ECS$  taking a value lower than the value shown on the  $x$ -axis. The black horizontal lines in Figure 3(b) show the 66% confidence limits [2.2 to 3.4K], or approximately  $2.8\pm 0.6$ K. Relative to the IPCC range of 1.5-4.5K, this constraint on  $ECS$  therefore reduces the uncertainty by about 60%. Indeed, even the 95% confidence limits from the emergent constraint [1.6 to 4.0K] fit well within the IPCC ‘likely’ range for  $ECS$ . Our constraint is therefore at odds with a suggestion that the lower 66% confidence limit for  $ECS$  could be as high as 3K<sup>27</sup>. If we instead use all 39 historical runs in the CMIP5 archive, we find a slightly weaker emergent relationship, but derive a very similar emergent constraint on  $ECS$  (Table ED2). The constraint is also robust to the choice of

observational dataset, and to whether or not the model global temperature is calculated just across the points where there were observations<sup>28</sup> (Table ED2, Figure ED2).

Our choice of window-width was informed by sensitivity studies in which the emergent constraint was calculated for a range of this parameter. Figure 4(a) shows the best estimate and 66% confidence limits on *ECS* as a function of the width of the de-trending window. Our best-estimate is relatively insensitive to the chosen window width, but the 66% confidence limits show a greater sensitivity, with the minimum in uncertainty at a window width of about 55 years (as used in the analysis above). As Figure ED3 shows, at this optimum window-width the best-fit gradient of the emergent relationship between *ECS* and  $\Psi$  (=12.1) is also very close to our theory-predicted value of  $\sqrt{2} Q_{2xCO_2} / \sigma_Q$  (=12.2). This might be expected if this window length optimally separates forced trend from variability.

Figure 4(b) shows the probability of *ECS*>4K and *ECS*<1.5K as a function of window width. For comparison, the IPCC ‘likely’ range of 1.5-4.5K implies a 25% probability of *ECS*>4K, and a 16% probability of *ECS*<1.5K. At the optimum window width of 55 years, both probabilities are close to their minimum values of less than 2.5%. Our emergent constraint therefore greatly reduces the uncertainty in the *ECS* value of the Earth’s climate, implying a less than 1 in 40 chance of *ECS*>4K, and renewing hope that we may yet be able to avoid global warming exceeding 2K.

## References

1. Collins, M., R. Knutti, et al. Long-term Climate Change: Projections, Commitments and Irreversibility. In: *Climate Change 2013: The Physical Science Basis. Contribution of Working Group I to the Fifth Assessment Report of the Intergovernmental Panel on Climate Change* [Stocker, T.F., D. Qin, G.-K. Plattner, M. Tignor, S.K. Allen, J. Boschung, A. Nauels, Y. Xia, V. Bex and P.M. Midgley (eds.)]. Cambridge University Press, Cambridge, UK and New York, NY, USA (2013).
2. Hall, A. and Qu, X. Using the current seasonal cycle to constrain snow albedo feedback in future climate change. *Geophysical Research Letters*, 33, L03502 (2006).
3. Morice, C.P., et al. Quantifying uncertainties in global and regional temperature change using an ensemble of observational estimates: the HadCRUT4 dataset. *Journal of Geophysical Research*, 117, D08101 (2012).
4. Knutti, R., et al. Beyond equilibrium climate sensitivity. *Nature Geoscience*, doi: 10.1038/NGEO3017 (2017).
5. Gregory, J. M., et al. An observationally based estimate of the climate sensitivity. *J. Climate*, 15, 3117–3121 (2002).
6. Forster, P. M., et al.. Evaluating adjusted forcing and model spread for historical and future scenarios in the CMIP5 generation of climate models. *J. Geophys. Res. Atmos.*, 118, doi:10.1002/jgrd.50174 (2013).
7. Gregory, J.M., Andrews, T. Variation in climate sensitivity and feedback parameters during the historical period. *Geophysical Research Letters*, doi:10.1002/2016GL068406 (2016).
8. Forster, P.M. Inference of climate sensitivity from analysis of Earth's radiation budget. *Annual Reviews*, 44, 85-106 (2016).
9. Armour, K. C. Energy budget constraints on climate sensitivity in light of inconstant climate feedbacks. *Nature Climate Change*, 7, 331–335 (2017).
10. Annan, J. D., Hargreaves, J.C. Using multiple observationally-based constraints to estimate climate sensitivity. *Geophysical. Research Letters*, 33, L06704 (2006)
11. Cox, P.M., et al. Sensitivity of tropical carbon to climate change constrained by carbon dioxide variability. *Nature*, 494, 341–344 (2013).
12. Wenzel, S., et al.. Projected land photosynthesis constrained by changes in the seasonal cycle of atmospheric CO<sub>2</sub>. *Nature*, 538, 499–5 (2016).
13. Hasselmann, K. Stochastic climate models. I. Theory. *Tellus*, 28, 473-485 (1976).
14. MacMynowski, D.G. et al. The frequency response of temperature and precipitation in a climate model. *Geophysical Research Letters*, 38, L16711 (2011).

15. Caldeira, K., Myhrvold, N.P. Projections of the pace of warming following an abrupt increase in atmospheric carbon dioxide concentration. *Environ. Res. Lett.*, 8, 034039 (2013).
16. Geoffroy, O., *et al.*. Transient Climate Response in a Two-Layer Energy-Balance Model. Part I: Analytical Solution and Parameter Calibration Using CMIP5 AOGCM Experiments. *Journal of Climate*, 26, 1841–1857, doi:10.1175/JCLI-D-12-00195.1 (2013).
17. Flato, G., J. Marotzke, *et al.* Evaluation of Climate Models. In: *Climate Change 2013: The Physical Science Basis. Contribution of Working Group I to the Fifth Assessment Report of the Intergovernmental Panel on Climate Change* [Stocker, T.F., D. Qin, G.-K. Plattner, M. Tignor, S.K. Allen, J. Boschung, A. Nauels, Y. Xia, V. Bex and P.M. Midgley (eds.)]. Cambridge University Press, Cambridge, United Kingdom and New York, NY, USA (2013).
18. Leith, C. E.. Climate response and fluctuation dissipation. *Journal of Atmospheric Science.*, 32, 2022–2026 (1975).
19. Taylor, K.E., Stouffer, R.J., Meehl, G.A. An overview of CMIP5 and the experiment design. *Bull. Amer. Meteor. Soc.*, 93, 485-498 (2012).
20. Andrews, T., *et al.* Forcing, feedbacks and climate sensitivity in CMIP5 coupled atmosphere-ocean models. *Geophysical Research Letters*, 39, L09712 (2012).
21. Kiehl, J.T. Twentieth century climate model response and climate sensitivity. *Geophysical Research Letters*, 10.1029/2007GL031383 (2007).
22. Lenton, T.M., *et al.* Tipping elements in the Earth’s climate system. *Proc. Nat. Acad. Sci.*, 105, 786-793 (2008).
23. Scheffer, M., *et al.* Early-warning signals for critical transitions. *Nature*, 461, 53-59 (2009).
24. Otto, A., *et al.* Energy budget constraints on climate response. *Nature Geoscience*, 6, 415-416 (2013).
25. Lewis, N. & Curry, J.A. The implications for climate sensitivity of AR5 forcing and heat uptake estimates. *Climate Dynamics*, 45, 1009-1023 (2015).
26. Marvel, K., *et al.*. Implications for climate sensitivity from the response to individual forcings. *Nature Climate Change*, 6, 386–389 (2016).
27. Sherwood, S. C., Bony, S., J.-L. Dufresne, J.-L. Spread in model climate sensitivity traced to atmospheric convective mixing. *Nature*, 505, 37–42, doi:10.1038/nature12829 (2014).
28. Cowtan, K., Way, R.G. Coverage bias in the HadCRUT4 temperature series and its impact on recent temperature trends. *Q. J. R. Meteorol. Soc.*, 140, 1935–1944 (2014).



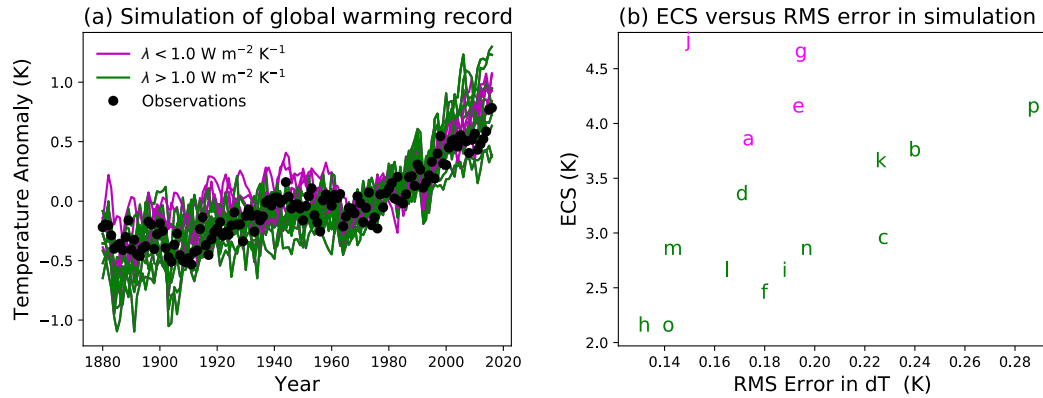


**Figure 1: Historical global warming.** (a) Simulated change in global temperature from 16 CMIP5 models (coloured lines), compared to the global temperature anomaly from the HadCRUT4 dataset (black dots). The anomalies are relative to a baseline period of 1961-90. The model lines are colour-coded with lower sensitivity models ( $\lambda > 1 \text{ W m}^{-2} \text{ K}^{-1}$ ) shown by green lines, and higher sensitivity models ( $\lambda < 1 \text{ W m}^{-2} \text{ K}^{-1}$ ) shown by magenta lines. (b) Scatter plot of each model's Equilibrium Climate Sensitivity (*ECS*) against the root-mean-square error in the fit of each model to the observational record.

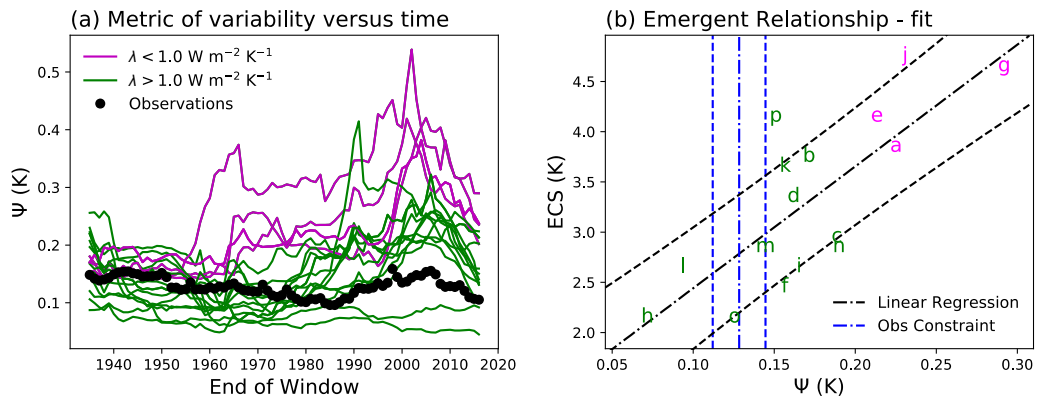


**Figure 2: Metric of global mean temperature variability.** (a)  $\Psi$  metric of variability versus time, from the CMIP5 models (coloured lines), and the HadCRUT4 observational data (black circles). The  $\Psi$  values are calculated for windows of width 55-years, after linear de-trending in each window. These 55-year windows are shown for different end times. As in figure 1, lower sensitivity models ( $\lambda > 1 \text{ W m}^{-2} \text{ K}^{-1}$ ) are shown by green lines, and higher sensitivity models ( $\lambda < 1 \text{ W m}^{-2} \text{ K}^{-1}$ ) are shown by magenta lines. (b) Emergent Relationship between the Equilibrium Climate Sensitivity (*ECS*) and the  $\Psi$  metric. The black dot-dashed line shows the best-fit linear regression across the model ensemble, with the prediction error for the fit given by the black dashed lines (see Methods). The vertical blue lines show the observational constraint from the HadCRUT4 observations: mean (dot-dashed line), and mean plus and minus one standard deviation (dashed lines).

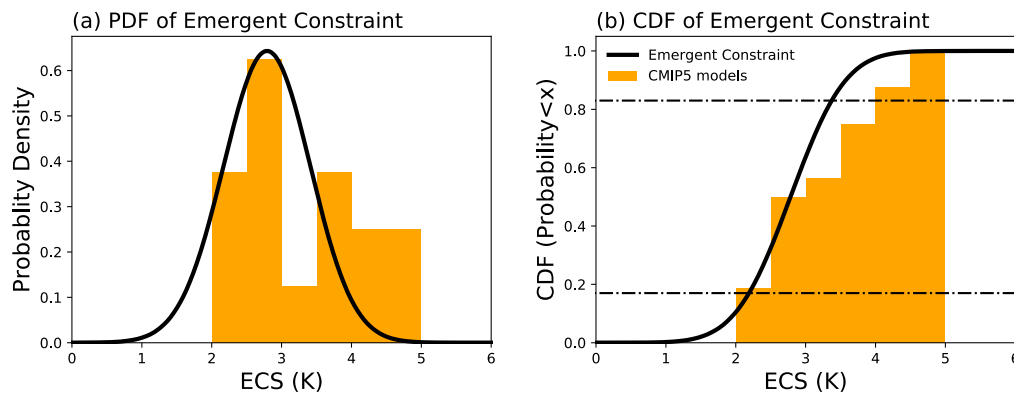


**Figure 3: Emergent Constraint on the Equilibrium Climate Sensitivity ( $ECS$ ).** Panel (a) shows the Probability Density Function (PDF) for  $ECS$  and panel (b) shows the related Cumulative Density Function (CDF). The horizontal dash-dot lines show the 66% confidence limits on the CDF plot. The orange histograms (both panels) show the prior distributions that arise from equal weighting of the CMIP5 models in 0.5K bins.

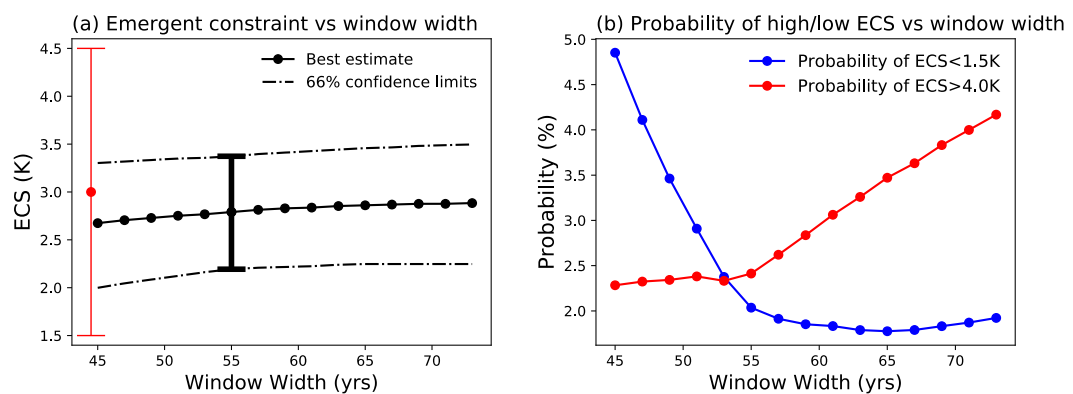


**Figure 4: Sensitivity of the Emergent Constraint on  $ECS$  to window width.** (a) Central estimate and 66% confidence limits. The thick black bar shows the minimum uncertainty at a window width of 55 years and the red bar shows the equivalent ‘likely’ IPCC range of 1.5-4.5K. (b) Probability of  $ECS > 4K$  (red line and symbols) and  $ECS < 1.5K$  (blue line and symbols).

## Extended Data

	Model	$\lambda$ ( $\text{Wm}^{-2} \text{K}^{-1}$ )	ECS (K)	$Q_{2xCO_2}/\sigma_N$	$\Psi$ (K)
a	ACCESS1-0	0.8	3.8	8.5	0.22
b	CanESM2	1.0	3.7	8.3	0.17
c	CCSM4	1.2	2.9	7.3	0.19
d	CNRM-CM5	1.1	3.3	8.7	0.16
e	CSIRO-MK3-6-0	0.6	4.1	6.1	0.21
f	GFDL-ESM2M	1.4	2.4	5.9	0.15
g	HadGEM2-ES	0.6	4.6	7.8	0.29
h	inmcm4	1.4	2.1	11.9	0.07
i	IPSL-CM5B-LR	1.0	2.6	7.2	0.16
j	MIROC-ESM	0.9	4.7	11.7	0.23
k	MPI-ESM-LR	1.1	3.6	11.9	0.15
l	MRI-CGCM3	1.2	2.6	9.3	0.09
m	NorESM1-M	1.1	2.8	7.8	0.14
n	bcc-csm1-1	1.1	2.8	6.9	0.19
o	GISS-E2-R	1.8	2.1	11.1	0.12
p	BNU-ESM	1.0	4.1	8.0	0.15
f*	GFDL-ESM2G	1.3	2.4	7.1	0.20
f'	GFDL-CM3	0.8	4.0	6.7	0.36
j*	IPSL-CM5A-LR	0.8	4.1	8.6	0.20
j*	MIROC5	1.5	2.7	10.2	0.23
n*	bcc-csm1-1-m	1.2	2.9	7.4	0.14
o*	GISS-E2-H	1.7	2.3	11.8	0.10

**Table ED1:** Earth System Models used in this study, as provided by the CMIP5 project<sup>19</sup>. The first column shows the symbol used for each model in all figures. The third and fourth columns list the Climate Feedback Factor ( $\lambda$ ) and the Equilibrium Climate Sensitivity (ECS) values, as given in IPCC AR5 Table 9.5. The fifth and sixth columns show statistics calculated in this study for the period 1880-2016 and using a window-width of 55 years. The fifth column shows the ratio of the radiative forcing due to doubling CO<sub>2</sub> ( $Q_{2xCO_2}$ ) to the standard deviation of the net top-of-atmosphere flux ( $\sigma_N$ ); and the sixth column shows the time-mean  $\Psi$  statistic for each model.

Observational Dataset	Obs. Constraint on $\Psi$ (K)	Number of Models	Best estimate ECS (K)	'Likely' range ECS (K)
HadCRUT4	0.13 +/- 0.016	16	2.79	2.19 - 3.37
NOAA	0.16 +/- 0.034	16	3.13	2.45 - 3.81
Berkeley Earth	0.13 +/- 0.021	16	2.79	2.16 - 3.39
GISSTEMP	0.12 +/- 0.025	16	2.66	2.00 - 3.28
ALL	0.13 +/- 0.029	16	2.85	2.18 - 3.49
HadCRUT4	0.13 +/- 0.016	16; filtered	2.82	2.19 - 3.43
HadCRUT4	0.13 +/- 0.016	22	2.82	2.16 - 3.47
HadCRUT4	0.13 +/- 0.016	39	2.96	2.34 - 3.56

**Table ED2:** Robustness of the Emergent Constraint to the choice of observational dataset and model ensemble. The 'ALL' dataset takes the mean and standard deviation of the  $\Psi$  values for all 4 global-mean temperature datasets (by concatenating the individual  $\Psi$  time-series). The 'filtered' model output calculates area-mean values of temperature just using the points where there are observations in the HadCRUT4 dataset<sup>27</sup>. All cases analyse 1880-2016 and use a 55-year window width.

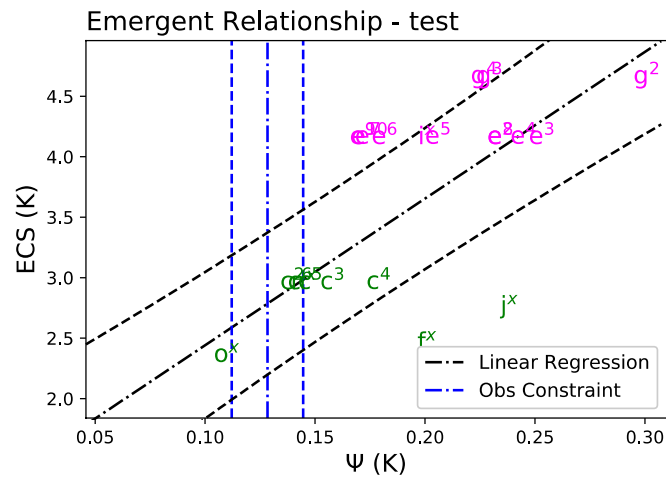


**Figure ED1:** Test of emergent relationship against models not used in the calibration. The test-set includes additional models from some climate centres (labelled ‘f<sup>x</sup>’, ‘f’ etc.), and initial condition ensembles with particular models (labelled ‘c<sup>2</sup>’, ‘c<sup>3</sup>’ etc.). The black dot-dashed line shows the best-fit linear regression across the model ensemble, with the prediction error for the fit given by the black dashed lines (see Methods). The vertical blue lines show the observational constraint from the HadCRUT4 observations: mean (dot-dashed line), and mean plus and minus one standard deviation (dashed lines).

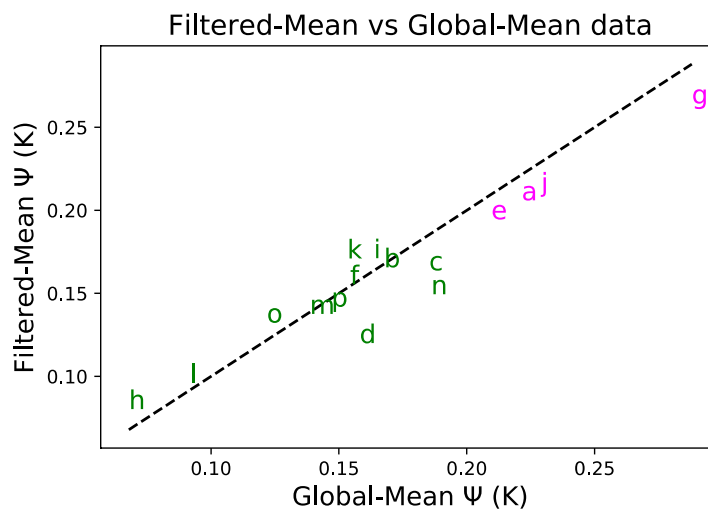


**Figure ED2:** Comparison of  $\Psi$  statistics for the 16 CMIP5 models from ‘filtered-mean’ temperature and global-mean temperature. The filtered model output calculates area-mean values of temperature just using the points where there are observations in the HadCRUT4 dataset. All cases analyse 1880-2016 and use a 55-year window width. The dotted line is the 1:1 line.

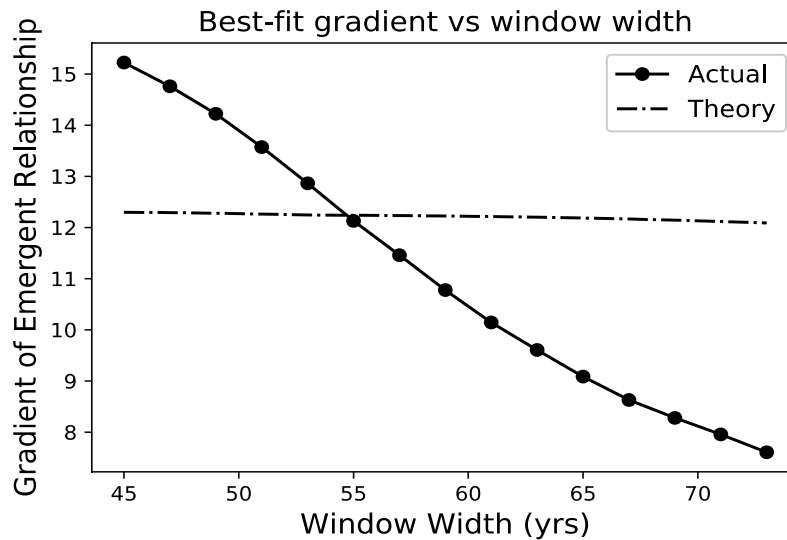


**Figure ED3:** Gradient of emergent relationship between  $ECS$  and  $\Psi$  as a function of window width. The dotted line shows the gradient predicted with Equation (2) using the ensemble-mean value of  $Q_{2xCO_2}/\sigma_N$ . Note that the theory (dot-dash line) fits best at the optimal window-width of 55 years. All cases here analyse 1880-2016 and use the 16-model ensemble.

**Acknowledgements.** This work was supported by the European Research Council (ERC) – ECCLES project, grant agreement number 742472 (P.C.); the EU Horizon 2020 Research Programme - CRESCENDO project, grant agreement number 641816 (P.C., M.W.); the EPSRC-funded ReCoVER project (M.W.); and the NERC CEH National Capability fund (C.H.). We also acknowledge the World Climate Research Programme's Working Group on Coupled Modelling, which is responsible for CMIP, and we thank the climate modelling groups (listed in Table ED1 of this paper) for producing and making available their model output.

**Author Contributions.** All authors collaboratively designed the study and contributed to the manuscript. P.M.C. led the study and drafted the manuscript. C.H. was the lead on the time-series data for the CMIP5 models. M.W. led on the theoretical analysis.

**Author Information.** Reprints and permissions information is available at [www.nature.com/reprints](http://www.nature.com/reprints). The authors declare no competing financial interests. Readers are

welcome to comment on the online version of the paper. Correspondence and requests for materials should be addressed to P.M.C. (p.m.cox@exeter.ac.uk)

## Methods

### 1 Theoretical Basis for the Emergent Relationship

We hypothesise that Equation (1) (the ‘Hasselmann Model’) is a reasonable approximation to the short-term variability of the global mean temperature anomaly ( $\Delta T$ ):

$$C \frac{d\Delta T}{dt} + \lambda \Delta T = Q$$

If trends arising from net radiative forcing and ocean heat uptake can be successfully removed, the net radiative forcing term ( $Q$ ) can be approximated by white noise. Under these circumstances, Equation (1) is essentially the Ornstein-Uhlenbeck equation which describes Brownian motion, and has standard solutions (e.g. see [https://en.wikipedia.org/wiki/Ornstein-Uhlenbeck\\_process](https://en.wikipedia.org/wiki/Ornstein-Uhlenbeck_process)) for the lag-1 autocorrelation of the temperature:

$$\alpha_{1T} = \exp\left\{-\frac{\lambda}{C}\right\}$$

and the ratio of the variances of  $T$  and  $Q$ :

$$\frac{\sigma_T^2}{\sigma_Q^2} = \frac{1}{2\lambda C}$$

These two equations can be combined to eliminate the unknown heat capacity ( $C$ ) and therefore to provide an expression for the climate feedback factor ( $\lambda$ ):

$$\lambda = \left\{\frac{\sigma_Q}{\sigma_T}\right\} \sqrt{-\frac{1}{2} \log_e \alpha_{1T}}$$

The Equilibrium Climate Sensitivity ( $ECS$ ) and  $\lambda$  are inversely related, with a constant of proportionality which is the radiative forcing due to doubling of atmospheric  $CO_2$  ( $Q_{2xCO_2}$ ):

$ECS = Q_{2xCO_2}/\lambda$ . Thus, we can also derive an expression for  $ECS$  in terms of the variability of  $T$  and  $Q$ :

$$ECS = Q_{2xCO_2} \left\{\frac{\sigma_T}{\sigma_Q}\right\} \sqrt{\frac{2}{-\log_e \alpha_{1T}}}$$

## 2 Least Squares Linear Regression

Least Squares linear regressions were calculated based on well-established formulae (see for example <http://mathworld.wolfram.com/LeastSquaresFitting.html>). The linear regression,  $f_n$ , between a time-series given by  $y_n$  and a time-series given by  $x_n$  is defined by a gradient  $b$  and intercept  $a$ :

$$f_n = a + b x_n$$

Minimising the least squares error for  $y_n$  involves minimising:

$$s^2 = \frac{1}{N-2} \sum_{n=1}^N \{y_n - f_n\}^2$$

where  $N$  is the number of data points in each time-series. In this case, the best-fit gradient is given by:

$$\bar{b} = \frac{\sigma_{xy}^2}{\sigma_x^2}$$

Here  $\sigma_x^2 = \sum_{n=1}^N \{x_n - \bar{x}\}^2 / N$  is the variance of  $x_n$ , and  $\sigma_{xy}^2 = \sum_{n=1}^N \{x_n - \bar{x}\} \{y_n - \bar{y}\} / N$  is the covariance of the  $x_n$  and  $y_n$  time-series - with means of  $\bar{x}$  and  $\bar{y}$  respectively.

The standard error of  $b$  is given by:

$$\sigma_b = \frac{s}{\sigma_x \sqrt{N}}$$

which defines a Gaussian Probability Density for  $b$ :

$$P(b) = \frac{1}{\sqrt{2\pi\sigma_b^2}} \exp\left\{-\frac{(b - \bar{b})^2}{2\sigma_b^2}\right\}$$

Finally, the ‘‘Prediction Error’’ of the regression is the following function of  $x$ :

$$\sigma_f(x) = s \sqrt{1 + \frac{1}{N} + \frac{\{x - \bar{x}\}^2}{N\sigma_x^2}}$$

This expression defines contours of equal probability density around the best-fit linear regression, that represent the probability density of  $y$  given  $x$ :

$$P\{y|x\} = \frac{1}{\sqrt{2\pi\sigma_f^2}} \exp\left\{-\frac{(y - f(x))^2}{2\sigma_f^2}\right\}$$

where  $\sigma_f = \sigma_f(x)$ , as described above.

### 3 Calculation of Probability Density Function for *ECS*

The emergent constraint derived in this study is a linear regression across the CMIP5 models between the Equilibrium Climate Sensitivity (*ECS*), and the  $\Psi$  statistic of the de-trended global temperature. In the context of the least squares linear regression presented above, *ECS* is equivalent to  $y$ , and  $\Psi$  is equivalent to  $x$ . The linear regression therefore provides an equation for the probability of *ECS* given  $\Psi$  (i.e. the equation for  $P\{y|x\}$  above). In addition, the  $\Psi$  statistic calculated from the de-trended observational dataset provides an observation-based PDF for  $\Psi$ . Given these two PDFs,  $P\{ECS|\Psi\}$  and  $P(\Psi)$ , the PDF for *ECS* is calculated by numerically integrating:

$$P(ECS) = \int_{-\infty}^{\infty} P\{ECS|\Psi\} P(\Psi) d\Psi$$

**Data availability:** The datasets generated during the current study are available from the corresponding author on reasonable request.

**Code availability:** The Python code used to produce the figures in this paper is available from the corresponding author on reasonable request.